Time-resolved photoluminescence microscopy combined with X-Ray analysis and Raman spectroscopies sheds light on the imperfect synthesis of historical cadmium pigments

Marta Ghirardello[1,*], Sara Mosca[1], Javier Marti-Rujas[2,†], Luca Nardo[3], Aviva Burnstock[4], Austin Nevin[5], Maria Bondani[6], Lucia Toniolo[7], Gianluca Valentini[1] and Daniela Comelli[1]

1 Physics Department, Politecnico di Milano, Piazza Leonardo da Vinci, 20133 Milano, Italy;
2 Chemistry, Materials and Chemical Engineering "Giulio Natta" Department, Politecnico di Milano, Via L.Mancinelli 7, 20133, Milano, Italy;
3 Department of Science and High Technology, University of Insubria, Via Valleggio 11, 22100, Como, Italy;
4 The Courtauld Institute of Art, Department of Conservation and Technology, Somerset House Strand, London London WC2R ORN, United Kingdom;
5 Institute for Photonics and Nanotechnologies, IFN-CNR, Piazza Leonardo da Vinci, 20133 Milano, Italy;
6 Institute for Photonics and Nanotechnologies, IFN-CNR, Via Valleggio 11, I-22100 Como, Italy;
7 Chemistry, Materials and Chemical Engineering "Giulio Natta" Department, Politecnico di Milano, Piazza Leonardo da Vinci, 20133, Milano, Italy;

* Correspondence: marta.ghirardello@polimi.it;
† Current address: Departament de Geologia, Universitat Autonoma de Barcelona, 08193 Bellaterra, Spain

ABSTRACT: Recent studies have shown that modern pigments produced after the Second Industrial Revolution are complex systems characterized by a high level of heterogeneities. Therefore, it is fundamental to adopt a multi-analytical approach and highly-sensitive methods to characterize the impurities present within pigments. In this work we propose time-resolved and spectrally-resolved photoluminescence (PL) microscopy for the mapping of luminescent crystal defects and impurities in historical cadmium-based pigments. PL analysis is complemented by X-ray diffraction, X-ray fluorescence, Raman spectroscopies and Scanning Electron Microscopy to determine the chemical composition and crystal structure of samples. The study highlights the heterogeneous and complex nature of historical samples that can be associated with the imperfect manufacturing processes tested during the period between the 1850s and 1950s. The results also allow us to speculate on a range of synthesis processes. Since it is recognized that the stability of paints can be related to pigments synthesis, this research paves the way to a wider study on the relationship between synthesis methods and deterioration of cadmium pigments and paints. This rapid and immediate approach using PL can be applied to other semiconductor pigments and real case studies.

The improvement in material synthesis methods from the end of the 19th century to the beginning of the 20th century, revolutionized artists' colour palettes with the introduction of industrially-manufactured coloured pigments. Many of these new materials were opaque and had high tinting strength, so that they were preferred to traditional artist's materials and include cadmium-based yellows[1]. Recent research has shown that many modern pigments, produced with non-refined and constantly evolving processes, are complex systems, with substantial heterogeneities. Illustrative examples of the complex chemistry of pigments include studies on lead chromate[2,3], zinc oxide[4,5] and HgS-based pigments[6,7], where it has been demonstrated that, beside the characterization of the bulk properties of historical pigments, it is essential to examine their heterogeneity with highly-sensitive methods. Spectroscopic methods, applied on the micro-scale and based on synchrotron radiation[3], have allowed researchers to elucidate the alteration processes of chrome yellow and the distribution of the degradation products in thin superficial paint layers. Equally, high-resolution nano-probe X-ray fluorescence has been applied to map metal impurities in submicron particles of zinc white paints, providing insights into the fabrication and chemical reactivity of paint[4]. Bertrand et al.[5] have shown how historical zinc white powders have a homogeneous photoluminescence (PL) when considering the bulk emission and an inhomogeneous emission on the sub-micrometer scale.

In this context, PL analyses are sensitive and capable of detecting traces of luminescent materials on the microscopic level[5,8,9]. Bellei et al.[8] have shown how time-resolved and spectrally-resolved PL microscopies can be effectively employed for the detection of luminescent centers, ascribed to transitional metal ions in ZnS

crystal matrix of historical samples of lithopone. On the basis of this research, a novel microscopy setup capable of achieving a full characterization of the PL emission in terms of both spectral and temporal emission properties has been developed.[9] The microscope system relies on a time-gated camera, which combines multi-spectral and lifetime detection at different lifetime ranges, spanning from few nanoseconds to hundreds of microseconds. This wide temporal range allows probing the emissions of modern semiconductor pigments, either occurring upon direct recombination or mediated by shallow and deep electron trapping.

In this study, we propose the application of the time-resolved PL microscopy approach to characterize the luminescent impurities present in historical cadmium based-semiconductor pigments. The aim of the work is to use the photo-physical and chemical properties of samples to illustrate the wide range of methods used to produce cadmium yellow pigments from the end of the 19th to the beginning of the 20th C. Since historical pigments were produced with non-refined methods, the presence of contaminants, and leftovers of manufacturing[10,11] or fillers needs to be investigated. Therefore, we adopted a combination of techniques working at different spatial scales. Microscopic analysis is combined with data acquired using a multi-analytical approach on bulk historical samples, comprising complementary techniques for elemental, morphological and molecular analysis (X-ray Fluorescence, X-ray Powder diffraction, Scanning Electron Microscopy and Raman spectroscopy).

Brief historical introduction on cadmium-based pigments

Cadmium was discovered by Stromeyer in 1817[1], but the development of cadmium compounds for commercial use as pigments followed the refinement of metal production methods in the mid-1840s[1]. Initially, a single shade of cadmium sulphide was made commercially available, with the misrepresentative name of 'cadmium yellow', since it corresponded to a medium yellow shade[1]. The high cost of raw materials limited the production of the pigment until the 1920s, when the refinement of manufacturing methods contributed to the spread of the production and availability of Cd-based pigments. Such implementations include the introduction of different shades composed of solid solutions of CdS with ZnS and CdSe[1,12], the development of the so called *cadmiopone* variety[1,12] and the improvement in the pigment stability[12]. A time diagram of pigment evolution is presented in Figure 1.

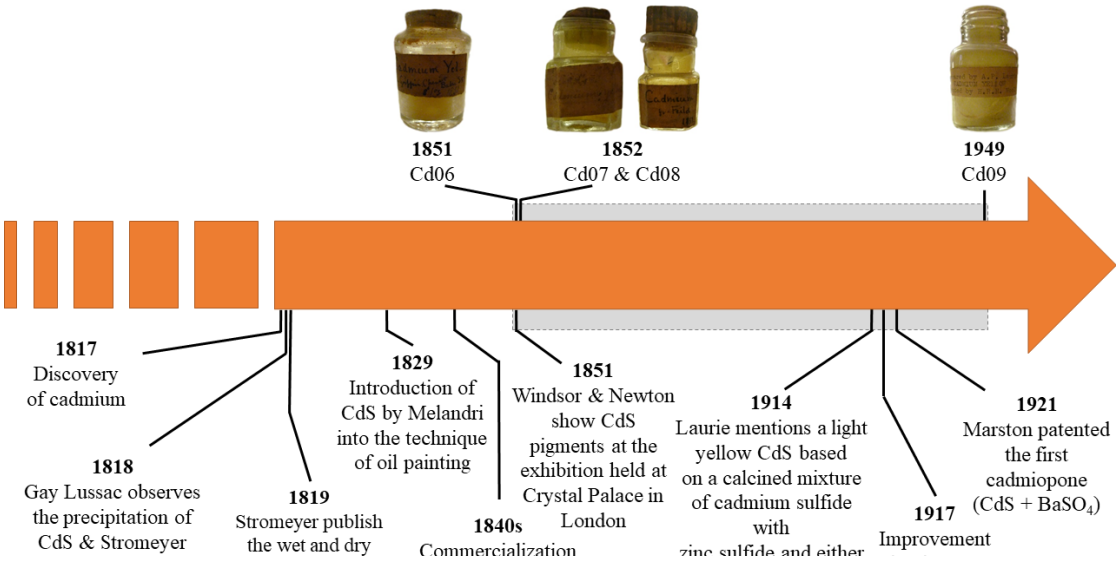

Figure 1. Evolution of synthesis methods of cadmium yellow pigments. The grey shaded area highlights the temporal interval covered by the historical pigments studied in this work.

Historically, there were two main methods to synthetize cadmium pigments: the 'dry' and the 'wet' processes[1,10,12,13]. The first method consists of calcining the cadmium metal or cadmium oxide/carbonate with sulphur at high temperature (300-500°) and in the absence of air, either in a stoichiometric mixture or in excess of sulphur. The time of reaction, temperature, purity of the reagent and presence of oxygen are all critical parameters affecting the quality of the final product. After complete reaction, the product is ground wet to give

the final shape and size to the powder[1]. The wet process involves precipitation of cadmium sulphide by reaction of a soluble cadmium salt (e.g. nitrate, chloride, sulphate, iodide, oxalate and carbonate) with a soluble sulphide (e.g. hydrogen, barium, sodium sulphide or a variety of thiosulfates). The precipitate is then washed and filtered, without undergoing any subsequent heating[1].

The pigments produced using these methods present two crystal forms. Calcination leads to the hexagonal matrix (corresponding to the Greenokite ore), while the historical wet method favors the formation of the cubic one (Hawleyite ore)[1]. In addition to these two forms, an amorphous phase may develop; however, it is unclear if this phase is generated by the grinding process, by reaction over time, or as a synthesis product[12].

Pigments based on cadmium sulphide have been widely employed by painters from impressionism on. However, these materials were used without concern about their chemical instability, which was often the cause of paint degradation and discoloration. Recent research[10,11,14–17] has shown that cadmium yellow undergoes a range of degradation processes, including chalking, fading, darkening or lightening. SR-based microscopic and spectroscopic techniques on paintings by Ensor, Van Gogh and Matisse[10,11,14–16] have partially elucidated the chemistry underlying the discolouration mechanisms of cadmium yellow. Nonetheless, the trigger mechanisms of the degradation pathways are still not fully understood, with studies suggesting that the stability of this paint depends on exposure to light and on the synthesis methods employed during pigment production[17], as has been shown for different systems including the iron-based pigment Prussian blue[18,19] and lead chromate[2,3].

Physically, cadmium sulphide belongs to the II-IV semiconductor group, with a large and pronounced band gap of 2.42 eV. Following photo-absorption, the fast near band-edge (NBE) emission has spectral features related to the pigment composition and crystal structure[20–22]. Moreover, the presence of two deep trap states (TS) located within the bandgap of the material, gives rise to an emission in the near infrared[21,22], with a lifetime in the order of microseconds[20]. The exact origin for the formation of these trap states is not fully understood, even though recent research attributes traps to cadmium vacancies[23].

MATERIALS AND METHODS

Nine powdered cadmium yellow-based pigments, dated between mid-1800 to mid-1900 from the archival collection of the Courtauld Institute of Art (London) were analyzed in this study[17]. In addition, two shades of commercial cadmium yellow (Kremer Pigmente GmbH & Co, Germany), available as pigment powders, were included in the analysis. The selected colors are Cadmium yellow light (Kp2) and Cadmium yellow dark (Kp4). For PL and Raman measurements, the samples were dispersed between two thin (~150 μm) and non-fluorescent microscope coverslips. All the other analyses were performed directly on powders.

Since the adopted techniques and procedures are published and are well established, a detailed description of the methods and measurements protocol is reported in Supplementary Information (SI), while here we limit the description to the most significant information.

X-Ray analysis and Raman spectroscopy

A portable X-ray Fluorescence (XRF) spectrometer (ELIO, XGLAB srl, Milan, Italy) was used for the qualitative analysis of the elements presents in the samples.
A benchtop X-Ray powder diffraction (XRPD) diffractometer (D2 PHASER, Bruker, Billerica, Massachusetts, USA), using the Bragg-Brentano geometry, was employed to identify the crystalline phase and to determine the degree of crystallinity of samples.
A Raman spectrometer[24], employing 785 nm laser excitation, was used to estimate the main chemical composition of pigment samples in an analysis point of 50 μm in later size. The identification of pigments was achieved through comparison with Raman spectra from published references[25,26].

PL spectroscopies

Steady-state laser induced PL spectroscopy was used to detect the spectral properties of the optical emission in the samples. The system[27] employed two different lasers sources working at different fluence values - a pulsed laser (CryLas FTSS 355-50, Crylas GmbH, Berlin, Germany) and a continuous laser source (DL-375-015, CrystaLaser, USA) - to promote NBE and TS emissions, respectively.
A picosecond Time-Correlated-Single-Photon-Counting (TCSPC) apparatus[28] was employed to detect the fast

decay kinetic of the NBE emission, while microsecond time-resolved photoluminescence (TRPL) spectroscopy[27] provided an evaluation of the TS emission decay kinetic of samples.

Scanning electron microscopy (SEM)

Scanning electron microscopy (SEM) was used to characterize the morphology and microstructure of samples. The system (ZEISS EVO 50EP), designed for high vacuum operation (pressure used 10^{-3} Pa) and employed at 20 kV acceleration voltage, has allowed us to achieve a spatial resolution of 1.2 nm for secondary electrons.

Conventional epifluorescence microscopy

A commercial optical microscope (Leica DM RE, Germany), equipped with a colour digital camera (NIKON D750, Tokyo, Japan) was employed for the observation of TS emissions in samples.

Time-resolved photoluminescence (TRPL) microscopy

The system, fully described elsewhere[9], allows the detection and the discrimination between NBE and TS emissions and the reconstruction of the related spectral and decay kinetic properties in each point of the sample surface. To provide an estimation of the size of heterogeneities and their relative abundance, spectral images were analysed in Matlab™. Following spatial calibration and the setting of proper intensity threshold factors, the diameters of local emitting centers were calculated by approximating them to circular spots, with a lateral resolution given by the system of 1.2 µm. The relative abundance of luminescent heterogeneities was determined by comparing the PL spectrum of a selected luminescent center (in the following quoted as reference spectrum) with that of all the other points in the field of view, by means of the spectral angle mapping algorithm[29]. The relative abundance of heterogeneities was then calculated as the ratio between the number of pixels with a spectrum similar to the reference one and the total number of pixels occupied by the sample.

RESULTS

The results of the preliminary characterization of the samples, in terms of elemental/molecular composition, crystal structure and particle dimensions, are summarized in Table 1 and data from XRF, XRPD, SEM and Raman are reported in SI.

Table 1. Samples data from XRF, XRPD, SEM and Raman spectroscopy together with the identification of the pigment and minor components. Crystal structure is indicated as hexagonal (h), cubic (c), orthorhombic (o), trigonal (t). Results of SEM analysis are reported in terms of mean particle size or size range. Raman bands are indicated as very strong (vs), strong (s), medium (m), weak (w), very weak (vw), broad (br) and shoulder (sh).

Sample	XRF	XRPD	SEM	Raman shift (cm^{-1})	Chemical Composition
Kp2	Cd, S, Zn, Ba, Sr	$Zn_xCd_{1-x}S$ (h) $BaSO_4$ (o)	-	214 vs, 304 s, 600 w ($Zn_xCd_{1-x}S$) 988 s ($BaSO_4$)	$Zn_xCd_{1-x}S$ (h) $BaSO_4$ (o, minor)
Kp4	Cd, S, Se (very traces), Ba, Sr	CdS (h) $BaSO_4$ (o)	-	211 vs, 300 s (CdS) 456 w, 988 s ($BaSO_4$)	CdS (h) $BaSO_4$ (o, minor)
Cd01	Cd, S	CdS (c/h) $CdCO_3$ (t)	0.26 µm	210 vs, 237 s (sh), 300 vs, 560 w, 600 m (CdS) 409 m, 487 vw, 1007 m, 1132 vw ($CaSO_4$) 1087 m ($CdCO_3$)	CdS (c/h) $CaSO_4$ (o, minor) $CdCO_3$ (t, minor)
Cd02	Cd, S, Zn, Ba, Sr	$Zn_xCd_{1-x}S$ (h) $BaSO_4$ (o)	0.24 - 1 µm	213 m, 306 vs, 610 w(br), 353 vw(sh) ($Zn_xCd_{1-x}S$) 456 w, 988 m ($BaSO_4$)	$Zn_xCd_{1-x}S$ (h) $BaSO_4$ (o, minor)
Cd03	Cd, S, Zn, Ba, Sr	$Zn_xCd_{1-x}S$ (h) $BaSO_4$ (o)	0.23 - 1 µm	213 m, 306 vs, 613 w(br), 353 w(sh) ($Zn_xCd_{1-x}S$) 456 w, 988 m ($BaSO_4$)	$Zn_xCd_{1-x}S$ (h) $BaSO_4$ (o, minor)
Cd04	Cd, S, Zn, Ba, Sr	$Zn_xCd_{1-x}S$ (h) $BaSO_4$ (o)	0.32 - 1 µm	214 m, 306 vs, 610 m(br), 353 m (sh) ($Zn_xCd_{1-x}S$) 456 w, 988 m ($BaSO_4$)	$Zn_xCd_{1-x}S$ (h) $BaSO_4$ (o, minor)
Cd05	Cd, S, Zn, Ba, Sr	$Zn_xCd_{1-x}S$ (h) $BaSO_4$ (o)	0.2 - 1 µm	214 m, 306 s, 615 w (br), 353 w(sh) ($Zn_xCd_{1-x}S$) 456 w, 988 m ($BaSO_4$)	$Zn_xCd_{1-x}S$ (h) $BaSO_4$ (o, minor)
Cd06	Cd, S, Zn (very traces)	CdS (h) CdS (c)	Fused grains	210 vs, 237 m (sh), 252 w(sh), 300 s, 347 m (sh), 363 w (sh), 560 w (sh), 600 m (br) (CdS)	CdS (h) CdS (c)
Cd07	Cd, S, Zn, Pb (traces)	CdS (c/h)	0.1 - 0.25 µm	214 m, 237 m (sh), 302 vs, 347 w(sh), 363 w(sh), 598 w(br) (CdS) 977 (br) ($PbSO_4$)	CdS (c/h) $PbSO_4$ (o, minor)
Cd08	Cd, S, Zn, Pb (traces)	CdS (c/h)	0.26 µm	214 m, 237 m, 302s, 347 w(sh), 363 w (sh), 598 w (CdS) 977 (br) ($PbSO_4$)	CdS (c/h) $PbSO_4$ (o, minor)
Cd09	Cd, S, Zn	$Zn_xCd_{1-x}S$ (h)	0.4 - 6 µm	no detection due to high fluorescence signal	$Zn_xCd_{1-x}S$ (h)

Elemental composition (XRF), crystal structure (XRPD) and particles dimensions (SEM)

Both historical and commercial samples contained main elements Cd, S and in some cases Zn. Ba, Sr and Pb were present in trace concentration.

From XRPD analyses, commercial Kp2 and Kp4 pigments were identified as solid solutions of hexagonal $Zn_xCd_{1-x}S$ and CdS, respectively, with the addition of barium sulphate as a minor component. Historical Cd01, Cd06, Cd07 and Cd08 were composed of CdS. Among them, the only sample that presented a clear crystal structure is Cd06, a mixture of hexagonal and cubic CdS. The broad XRPD peaks detected in the other three samples, with a mixed cubic/hexagonal pattern, suggest that they are ultra-fine pigments (submicron size) where both phases coexist[30]. The small size of pigment particles in these sample is indeed confirmed by SEM analysis, as discussed below.
In sample Cd01, XRPD measurements also identified cadmium carbonate. Samples from Cd02 to Cd05 and Cd09 showed a shift towards longer diffraction angles of the typical XRPD peaks of hexagonal CdS due to the presence of substitutional Zn ions. Hence, these samples are identified as mixtures of hexagonal $Zn_xCd_{1-x}S$, with an addition of barium sulphate (with the exception of Cd09, pure hexagonal $Zn_xCd_{1-x}S$).
Variation in particles size and shapes were revealed using SEM imaging. Most samples contained irregularly shaped particles, with an average size that varies from hundreds of nanometres to few microns. The largest grains were detected in sample Cd09 (mean size~6 μm). Samples Cd01, Cd07 and Cd08 contain spherical particles with the smallest dimension between 0.1 - 0.26 μm. Sample Cd06 appeared fused, with no clearly identifiable particles.

Micro-Raman spectroscopy
Commercial samples showed cadmium sulphide Raman modes at ~ 300 cm^{-1} (Longitudinal Optical modes, LO), and multi-phonon modes at ~ 210, 247, 370 cm^{-1} [21,31]. The red shift of the 210 cm^{-1} and 300 cm^{-1} modes in Kp2 is associated with the substitution of Zn ion in the crystal lattice, hence confirming the presence of solid solutions of $Zn_xCd_{1-x}S$.
No Raman bands were detected for sample Cd09 due to its overwhelming fluorescent emission. All other samples displayed the cadmium sulphide Raman modes at ~ 232-237 cm^{-1} (Transverse Optical phonon modes, TO), ~ 300 and 600 cm^{-1} (LO and 2LO respectively), and multi-phonon modes at ~ 210, 247, 336, 560 cm^{-1}. Moreover, the red shift of the 300 cm^{-1} (LO) and 600 cm^{-1} (2LO) modes, detected in samples from Cd02 to Cd05, is associated with the increasing of zinc content in the cadmium sulphide crystal, confirming the presence of solid solutions of $Zn_xCd_{1-x}S$.
Sample Cd06 showed both the Raman frequency pattern characteristic of hexagonal and cubic CdS crystal structures[31]. Equally, the presence of a consistent TO mode at 237 cm^{-1} in samples Cd01, Cd06, Cd07 and Cd08, characteristic of the CdS cubic structure, suggested the presence of this latter crystal phase[21].
Raman measurements highlighted the existence of heterogeneities of different nature. Samples Cd02 to Cd05 contain barium sulphate ($BaSO_4$, 453 and 988 cm^{-1}), Cd01 contains cadmium carbonate ($CdCO_3$, 1087 cm^{-1}) and calcium sulphate ($CaSO_4$, 409, 497, 1007 cm^{-1}), Cd07 and Cd08 contain traces of lead sulphate ($PbSO_4$, 977 cm^{-1}).

Bulk photoluminescence measurements
Samples Cd01, Cd07 and Cd08 did not show any detectable optical emission associated with either NBE or TS radiative recombination pathways. All the other historical samples, with the exception of Cd06 and Cd09, exhibited similar behaviour for NBE in terms of peak position (Figure 2): maxima are centred around 490 nm, in agreement with the PL spectral features of commercial sample Kp2 (based on $Zn_xCd_{1-x}S$) and PL results reported in the literature[20,21].
The emission peak of sample Cd06 is shifted towards longer wavelengths, similar to Kp4 (commercial CdS-based pigment). Moreover, it consists in the superposition of two distinguishable peaks (peaked at 510 and 530 nm), correlated with the presence of an intimate mixture of hexagonal and cubic CdS[21].

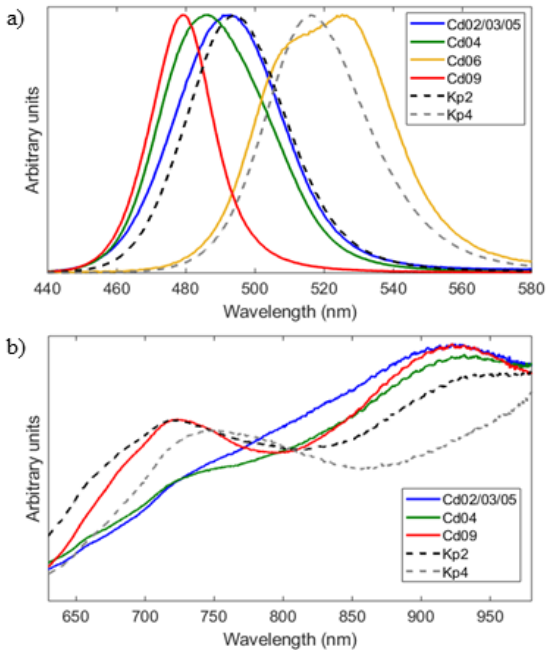

Figure 2. a) NBE and b) TS emission spectra; each curve is peak-normalized. For improve legibility, sample Cd02, Cd03 and Cd05, that exhibits almost the same emission in both NBE and TS, are represented by a single curve.

NBE decay kinetics showed a he order of 10 ps) in all historical and commercial samples, except for Cd04, that showed a longer lifetime (around 20 ps) of the first component. A full set of fitted data is reported in SI.

Commercial samples (Kp2 and Kp4) showed the typical TS emission of cadmium-based pigments, consisting of two broad peaks ascribed to two deep trap states in the bandgap of CdS and $Zn_xCd_{1-x}S$[21]. Recent research on commercial samples has shown that the emissions related to the first and the second deep trap state is expected in the range 680:750 nm and 880:1000 nm, respectively, depending on the fraction of substitutional zinc ions in the CdS crystal matrix[21]. The historical samples showed a different range of spectral emissions, instead (Figure 2). Cd06, characterized by a detectable NBE emission, showed no TS emission. All the other samples, with the exception of Cd09, presented a broad emission with a peak in the NIR portion of the spectrum (around 900 nm) and a small shoulder at shorter wavelength (around 725 nm). Sample Cd09 is the only historical sample characterized by two emission peaks, with a behaviour similar to the one of commercial sample KP2.
In terms of emission decay, TS emissions from all historical samples showed faster decay (mean effective lifetime of 10 μs) than that detected in commercial ones (mean effective lifetime of 27 μs). Full data are reported in SI.

Although the adopted PL device could not measure optical emission quantum yields, it is worth noting that, from a qualitative standpoint, all the samples, measured in the same experimental conditions, showed similar emission intensities. The only exceptions are constituted by Cd09, that has a much brighter NBE and TS optical emission than all other samples, and Cd06, that displays a weaker NBE emission and lacks a measurable TS emission. Detailed results are reported in SI.

Conventional PL microscopy and TRPL microscopy
Observation of samples with a conventional epi-fluorescence microscope (Figure 3) reveals that all luminescent historical samples present heterogeneities with significantly different TS optical emissions. Conversely, commercial KP2 and KP4 samples show a TS emission with only few heterogeneities that are spectrally similar to bulk emission. The results of TRPL microscopy studies of two samples (Cd04 and Cd09) is discussed here (TRPL microscopy data of all samples are available in SI).

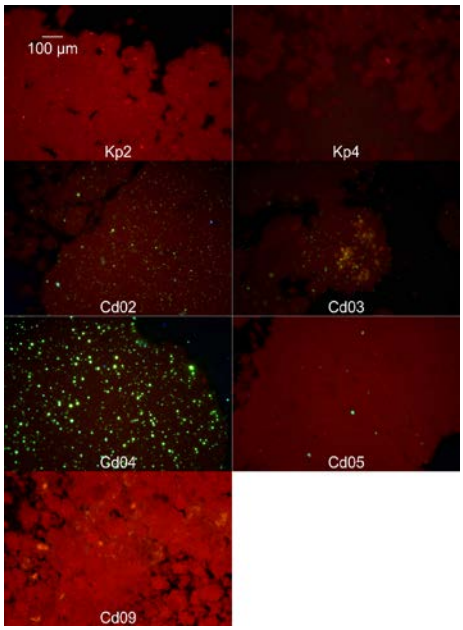

Figure 3. Images of the PL emission of historical samples following trap state recombination.

Sample Cd04 showed heterogeneities in both NBE (Figure 4a) and TS emissions (Figure 5a). On the nanosecond time scale the pigment exhibits, beside bulk NBE emission, some brighter spots (Figure 4b) with an emission shifted to slightly longer wavelength (Figure 4c). These have a lateral size ranging from the minimum detectable size to ~13 µm, with a median of the distribution of 3.7 µm. Based on spectral similarities, it is possible to estimate that the fraction of local heterogeneities in the sample area is close to 1.7%. It is likely that the detected luminescent heterogeneities are due to the presence of a second solid solution of $Zn_xCd_{1-x}S$ (minor component) with a lower concentration of zinc with respect to the $Zn_xCd_{1-x}S$ solid solution that is dominant in the sample.

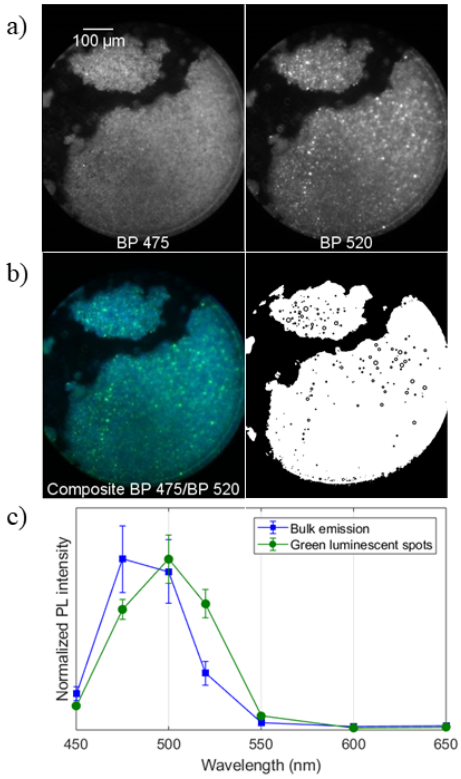

Figure 4. a) Spatial distribution of the nanosecond NBE PL emission of sample Cd04, detected in selected spectral bands (indicated by the label at the bottom of each image). b) False colour map created by combining nanosecond PL gated images in the two spectral bands (BP475: 455–495 nm (cyan), BP 520: 500–540 nm (green)) and false-colour image highlighting sample area (displayed as white) and luminescent centers (displayed as black circles). c) Mean PL spectra of the nanosecond emission detected in ROIs corresponding to bulk sample and to luminescent centers, with error bars reporting the standard deviation within each ROI.

On a microsecond timescale, beside the bulk TS emission beyond 850 nm ascribed to the deep TS emission of $Zn_xCd_{1-x}S$, Cd04 showed two types of heterogeneity (Figure 5a and b): (i) green and bright luminescent spots (emission peaked around 520 nm, Figure 5c) and (ii) infrared-luminescent spots (emission peaked at 750 nm, Figure 5c). The former has a maximum lateral size of ~24 µm and a relative abundance of 0.7 %, the latter a maximum lateral size of ~15 µm and a relative abundance of 0.2 %.

In terms of decay kinetics, the green luminescent spots exhibited a lifetime much shorter than the TS bulk emission, while infrared-luminescent centers showed a similar decay kinetic with respect to the bulk TS emission (Figure 5d). Finally, it is worth noting that the spatial heterogeneities detected on the nanosecond timescale did not coincide with those at microsecond timescales.

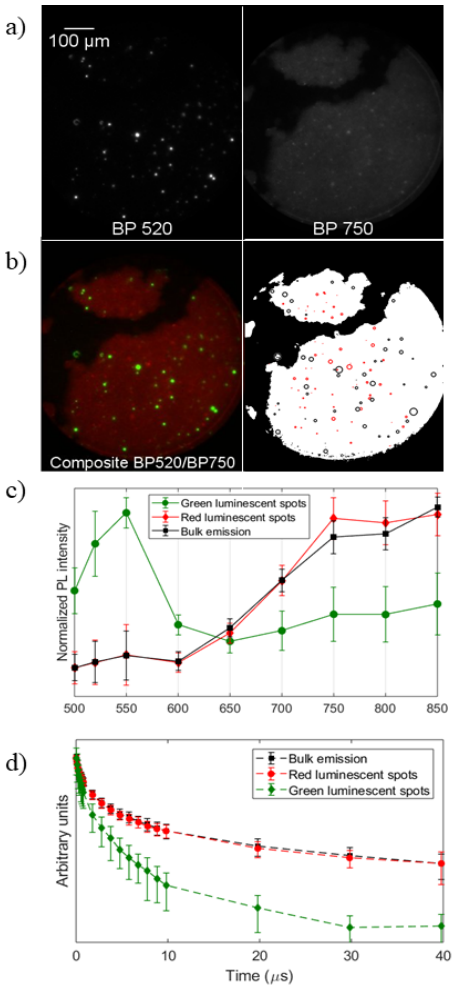

Figure 5. a) Spatial distribution of the microsecond TS PL emission, of sample Cd04 detected in selected spectral bands (indicated by the label at the bottom of each image). b) False colour map created by combining microsecond PL gated images in the two spectral bands (BP520: 500–540 nm (green), BP750: 730–770 nm (red)) and false-colour image highlighting the sample area (displayed as white) and the luminescent centers emitting at 520 nm (displayed as black circles) and at 750 nm (displayed as red circles). Reconstructed mean PL spectra (c) and decay kinetic (d) of the microsecond emission detected in ROIs corresponding to the bulk sample and to green and red luminescent centers, with error bars reporting the standard deviation within each ROI.

Similar spatial heterogeneities of the NBE and TS optical emission were detected in other historical samples, with some variation in their relative abundance and lateral size, as reported in Table 2.

Table 2. Central wavelength of the spectral band corresponding to maxima of the NBE and TS emission for the bulk sample ($\boldsymbol{\lambda_{BULK}}$) and for the detected heterogeneities ($\boldsymbol{\lambda_{HET}}$). For each type of luminescent heterogeneity, we report the estimate of the distribution of lateral size in terms of median (M) and maximum value (max) and the estimate of the relative abundance (r.a.). The minimum detectable size corresponds to the spatial resolution of the TRPL microscopy set-up, that is equal to 1.2 µm.

Sample	NBE				TS						
	λ_{BULK} (nm)	λ_{HET} (nm)	M/max (µm)	r.a.	λ_{BULK} (nm)	λ_{HET} (nm)	M/max (µm)	r.a.	λ_{HET}(nm)	M/max (µm)	r.a.
Cd02	475	520	2.8 / 21.8	0.2%	850	550	1.4 / 20.0	0.2%	700	1.4 / 6.6	0.1%
Cd03	475	500	7.7 / 11.0	5%	850	520	5.6 / 16.0	0.2%	750	3.0 / 4.9	1.8%
Cd04	475	520	3.7 /14.0	1.7%	850	520	8.6 / 24.0	0.7%	750	3.5 / 15.5	0.2%
Cd05	475	500	2.7 / 20.0	1.5%	850	-	-	-	-	-	-
Cd09	475	-	-	-	750	550	4.5 / 19.5	1.9%	-	-	-

Sample Cd09 showed a bright and homogeneous NBE emission (in terms of spectrum and decay kinetics). The TS emission revealed the existence of luminescent centers emitting in the spectral region centered at 550 nm (Figure 6a). Instead, this is the only sample characterized by a non-homogeneous behaviour of the decay kinetic of the bulk TS emission (centered at 750 nm), as is highlighted in the lifetime map displayed in Figure 6b. We remark that lifetime heterogeneities do not coincide spatially with the luminescent centers emitting at 550 nm.

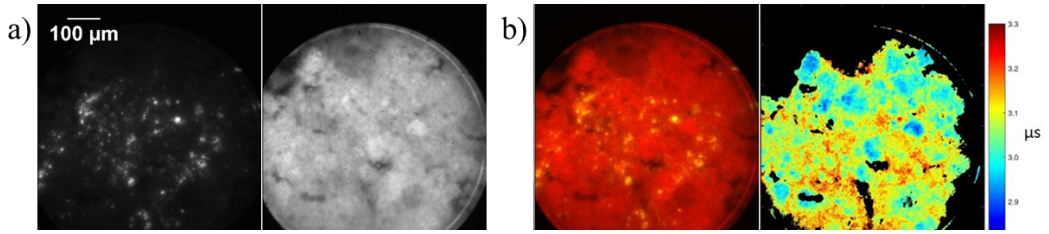

Figure 6. a) Spatial distribution of the microsecond TS PL emission of sample Cd09, detected in selected spectral bands (indicated by the label at the bottom of each image). b) False colour map created by combining microsecond PL gated images in the two spectral bands (BP550: 530–570 nm (yellow), BP750: 730–770 nm (red)) and lifetime map obtained performing a mono-exponential fit on a pixel-to-pixel basis in the temporal range from 0.2 to 10 µs.

DISCUSSION

The results of this study show clear differences in the chemical composition and crystal structure of historical pigment powders, which contained variable impurities. Whereas contemporary cadmium yellow pigments are composed of hexagonal $Zn_xCd_{1-x}S$ (Kp2) or CdS (Kp4), with minor amounts of barium sulfate, probably added as an extender, historical pigments were found to contain different compounds and exhibit different degrees of crystallinity. Samples Cd01, Cd06, Cd07 and Cd08 are all based on CdS and comprised either hexagonal and cubic structures, with a submicron size crystals (Cd01, Cd07, Cd08) or fused grains (Cd06). Samples Cd02 to Cd05 and Cd09 are composed of hexagonal solid solutions of $Zn_xCd_{1-x}S$, with different amount of zinc. Micrometric agglomerates are present, surrounded by smaller particles.

Impurities and extenders were identified in historical samples, such as residual traces of the starting reagent cadmium carbonate (in Cd01), of the extenders barium sulfate (in Cd02 to Cd05) and lead sulfate (in Cd07, Cd08) and of strontium impurities (in Cd02 to Cd05). The presence of zinc in CdS samples (Cd06, Cd07 and Cd08) can be related either to a very small fraction of $Zn_xCd_{1-x}S$, below the detection limit of XPRD, or to the manufacturing process of CdS. Indeed, pure cadmium sulphide is rare in nature, and is usually found as a coating on other minerals such as zinc Sphalerite or Wurtzite (ZnS)[1]. In this case, the presence of zinc can be related to residues of the extraction process.

In agreement with previous research on commercial and historical cadmium pigments[20,21,32], this study confirms that PL spectroscopy is extremely useful for the analysis of cadmium-based pigments. No optical emission was detected in pigments made of submicron particles (Cd01, Cd07, Cd08). Conversely, in pigments with larger crystals, the spectral position of the NBE emission is correlated with the chemical composition of yellow cadmium-based pigments, as already proposed by Rosi et al.[21], and is relatively unaffected by the presence of minor fractions of other compounds.

Whereas commercial samples showed typical emissions from the two deep TS of CdS and $Zn_xCd_{1-x}S$ based compounds[21], historical pigments, with the exception of sample Cd09, showed a single wide band centered in the NIR region. This suggests that in most of the analyzed historical samples the emission from the second deep TS is favoured with respect to the first one, implying that the mechanisms of electron trapping and trap de-excitation are different in these materials. Indeed, synthesis methods can account for the observed differences, since non-refined synthesis could introduce different defects and impurities in the crystal matrix.

Beyond bulk analysis, TRPL microscopy was highly effective in mapping the presence of many and different luminescent heterogeneities in historical samples. The spatial mapping of the spectral features of the NBE emission allows us to highlight that some of the historical samples (Cd03, Cd04 and Cd05) are intimate mixtures of two $Zn_xCd_{1-x}S$ compounds, with the minor component of the mixture occurring at concentrations below the limit of detection of XRPD and Raman bulk analyses. The spatial mapping of the TS emission demonstrates the presence of luminescent centers ascribed to impurities, substitutional ions or charged crystal defects. In samples from Cd02 to Cd04 and in Cd09, we detected long-lived (microsecond) luminescent centers with emission peaked at 500/550 nm. It is likely that the origin of this optical emission is due to local substitutional ions in the crystal matrix of $Zn_xCd_{1-x}S$, similar to the behaviour reported for historical ZnS-based pigments[8], or to substitutional ions in $BaSO_4$. This latter hypothesis is supported by the observation of the green luminescent centers only in historical samples with $BaSO_4$. For local heterogeneities emitting in the near-infrared, since their emission is slightly different from that of the bulk (mainly in terms of spectral features and, for sample Cd09, also in terms of decay kinetic), we speculate that they are related to deep trap states of $Zn_xCd_{1-x}S$, occurring at energies slightly higher than the ones present in the bulk material.

Hypotheses on the historical synthesis processes

Based on the results from the applied multi-analytical approach, the identification of the pigments crystal structure and size, the presence of additives and the mapping of impurities and crystal defects, we divide the analysed samples into five classes, listed in Table 3.

Table 1. Sample characteristics, composition, provenience, date and proposed production method. Crystal structure is indicated as hexagonal (h), cubic (c), orthorombic (o), trigonal (t).

Class/ samples		Chemical composition	Bottle label/ Year	Inferred synthesis process
1	Cd01	CdS (c/h) $CaSO_4$ (o) $CdCO_3$ (t)	'Cadmium yelorange' Leomertier Barbe LTD	Wet, finely ground, co-precipitation of $CdCO_3$ with sulphur and addition of calcium sulphate
2	Cd07	CdS (c/h) $PbSO_4$ (o)	Cadmium yellow (1852)	Wet, finely ground, early production of lighter shades with addition of lead white
	Cd08		Cadmium Field (1852)	
3	Cd06	CdS (h) CdS (c)	Cadmium Yel. Griffin 8th/03 (1851)	Wet, partially calcined with imperfect method
4	Cd02	$Zn_xCd_{1-x}S$ (h) $BaSO_4$ (o)	CdS yellow	Dry process with the addition of small amount of barium sulphate, possible early production of cadmiopone
	Cd03		Cd yellow	
	Cd04		Cd Lemon	
	Cd05		Cadmium yellow	
5	Cd09	$Zn_xCd_{1-x}S$ (h)	Prepared by A.P.Laurie Cadmium yellow (1949)	Dry process, well calcined

(1) The first class consists of sample Cd01. It is proposed that this pigment was synthetized using an imperfect wet process that formed a cubic crystalline phase. The product was then washed improperly (as indicated by the presence of residual starting reagent such as cadmium carbonate) and ground to reduce the particle size, converting the crystal phase to a mixture of cubic and hexagonal one[30]. No subsequent calcination process was performed. This led to a nano-crystalline pigment, with no photoluminescence.

(2) The second class consists of pigments (Cd07 and Cd08) with almost the same characteristic of class one, obtained with wet process and subsequently finely ground (submicron particles). Here, however, no residual starting reagent was found. Our hypothesis on the employed production method is corroborated by the production dates, which correspond to the first period of cadmium pigment development, where calcination (that leads to hexagonal crystal structure[30]) was not used. Moreover, the presence of lead sulphate suggests the addition of this extender to obtain lighter shades. Indeed, it is known that the early productions of lighter shades were obtained with the addition of lead-based white[1], without taking into account the potential instability deriving from the mixing of these two compounds.
(3) The third class consists of sample Cd06 only, a mixture of hexagonal and cubic cadmium sulphide. The presence of the two crystal structures may be due to mixing of more batches of pigments or to improper calcination. Since the date of the pigment is 1851, we deduce that it was synthetized following the first experiments on calcination of cadmium sulphide. It may be that the heating process was not completed, which is suggested by the presence of both the CdS polymorphs.
(4) The fourth class contains pigments based on cadmium zinc sulphide with the addition of barium sulphate. Since historically the solid solutions were introduced later and the degree of crystallinity is well defined, it is possible that these pigments were produced using a dry process and are more recent than the first two classes. The presence of impurities, highlighted by TRPL microscopy measurements, suggests a process that is not well refined for either cadmium sulphate or barium sulphate. In particular, sample Cd04 shows heterogeneities in both NBE and TS emission, with greater abundance and lager size compared to other pigments of this class.
(5) The last class consists in sample Cd09, based on hexagonal $Zn_xCd_{1-x}S$. Since it exhibits peculiar behaviour with an extremely bright emission, it might have been produced using a different method than those pigments in other classes.

CONCLUSIONS

Our results reveal the complexity and the significant heterogeneity of different cadmium yellow pigments synthetized between 1850 and 1950. The differences detected in samples, including their characteristic crystal structure and impurities, may be related to the different synthesis processes and recipes available in that period. The combination of a range of spectroscopic and microscopic methods has led to clear hypotheses on the synthesis methods used for the pigments. The identification of different crystal structures (hexagonal and cubic) related to the production processes (dry and wet) and the determination of additives or residual starting regents highlight the complex nature of the historical samples analysed. These findings were supported by time-gated PL microscopy, that revealed heterogeneous luminescent impurity traces present in each historical sample. These impurities can be ascribed to the imperfect manufacturing processes tested during the development of the synthesis of the pigment. In this context time resolved PL, compared to other methods capable of detecting local impurities and crystal defects (like Electron Paramagnetic Resonance spectroscopy[8])can be performed as a microscopy technique, and hence is useful for mapping luminescent heterogeneities on the microscale[9].
As a consequence of the heterogeneity in crystal structure and chemical composition of historical pigments, it is expected that these pigments may have different reactivity, and prone or resistant to degradation, as is occasionally reported in cadmium-based paints[10,11,14–16]. This research paves the way to a wider study on historical cadmium pigments and paints and on other semiconductor pigments, including important pigment archives, to elucidate the link between their physical and chemical properties and their tendency to degrade in paintings.

ASSOCIATED CONTENT

Supporting Information Available: images of archive pigment's bottles from the Courtauld Institute of Art, microscopic images and details on manufacture; detailed description of methods; XRF, XPRD, Micro Raman and bulk PL emission data; bulk PL decay kinetic and results of data fitting; selected sub-dataset of micro-time resolved photoluminescence microscopy.

REFERENCES

(1) Fiedler, I.; Bayard, M. A. *In Artists' Pigments. A Handbook of Their History and Characteristics*; Feller, R. L., Ed.; Cambridge University Press: Cambridge, 1986.

(2) Monico, L.; Van Der Snickt, G.; Janssens, K.; De Nolf, W.; Miliani, C.; Verbeeck, J.; Tian, H.; Tan, H.; Dik, J.; Radepont, M.; et al. *Anal. Chem.* **2011**, *83* (4), 1214–1223.

(3) Monico, L.; Van Der Snickt, G.; Janssens, K.; De Nolf, W.; Miliani, C.; Dik, J.; Radepont, M.; Hendriks, E.; Geldof, M.; Cotte, M. *Anal. Chem.* **2011**, *83* (4), 1224–1231.

(4) Casadio, F.; Rose, V. *Appl. Phys. A Mater. Sci. Process.* **2013**, *111* (1), 1–8.

(5) Bertrand, L.; Réfrégiers, M.; Berrie, B.; Échard, J.-P.; Thoury, M. *Analyst* **2013**, *138* (16), 4463.

(6) Cotte, M.; Susini, J.; Metrich, N.; Moscato, A.; Gratziu, C.; Bertagnini, A.; Pagano, M. *Anal. Chem.* **2006**, *78* (21), 7484–7492.

(7) Radepont, M.; de Nolf, W.; Janssens, K.; Van der Snickt, G.; Coquinot, Y.; Klaassen, L.; Cotte, M. *J. Anal. At. Spectrom.* **2011**, *26* (5), 959.

(8) Bellei, S.; Nevin, A.; Cesaratto, A.; Capogrosso, V.; Vezin, H.; Tokarski, C.; Valentini, G.; Comelli, D. *Anal. Chem.* **2015**, *87* (12), 6049–6056.

(9) Comelli, D.; Artesani, A.; Nevin, A.; Mosca, S.; Gonzalez, V.; Eveno, M.; Valentini, G. *Materials (Basel).* **2017**, *10* (11), 1–16.

(10) Van Der Snickt, G.; Dik, J.; Cotte, M.; Janssens, K.; Jaroszewicz, J.; De Nolf, W.; Groenewegen, J.; Van Der Loeff, L. *Anal. Chem.* **2009**, *81* (7), 2600–2610.

(11) Mass, J. L.; Opila, R.; Buckley, B.; Cotte, M.; Church, J.; Mehta, A. *Appl. Phys. A Mater. Sci. Process.* **2013**, *111* (1), 59–68.

(12) Eastaugh, N.; Walsh, V.; Siddall, R.; Chaplin, T. *Pigment Compendium: A Dictionary and Optical Microscopy of Historical Pigments.* Elsevier, Elsevier Butterworth-Heinemann, Oxford (2008).

(13) Van der Snickt, G. *James Ensor's Pigments Studied by Means of Portable and Synchrotron Radiation-Based X-Ray Techniques: Evolution, Context and Degradation,* Doctoral dissertation, University of Antwerp, Chemistry Departement, **2012**.

(14) Van Der Snickt, G.; Janssens, K.; Dik, J.; Nolf, W. De; Vanmeert, F.; Jaroszewicz, J.; Cotte, M.; Falkenberg, G. *Anal. Chem.* **2012**, *84* (23), 10221−10228.

(15) Mass, J.; Sedlmair, J.; Patterson, C. S.; Carson, D.; Buckley, B.; Hirschmugl, C. *Analyst* **2013**, *138* (20), 6032.

(16) Pouyet, E.; Cotte, M.; Fayard, B.; Salomé, M.; Meirer, F.; Mehta, A.; Uffelman, E. S.; Hull, A.; Vanmeert, F.; Kieffer, J.; et al. *Appl. Phys. A Mater. Sci. Process.* **2015**, *121* (3), 967–980.

(17) Leone, B.; Burnstock, A.; Jones, C.; Hallebeek, P.; Boon, J. J.; Keune, K. In *ICOM Committee for Conservation. Triennial meeting, 14th, The Hague, Netherlands*; James and James/Earthscan, 2005; Vol. 2, pp 803–813.

(18) Kirby, J.; Saunders, D. *Natl. Gall. Tech. Bull.* **2004**, *25*, 73–99.

(19) Samain, L.; Grandjean, F.; Long, G. J.; Martinetto, P.; Bordet, P.; Sanyova, J.; Strivay, D. *J. Synchrotron Radiat.* **2013**, *20* (3), 460–473.

(20) Cesaratto, A.; D'Andrea, C.; Nevin, A.; Valentini, G.; Tassone, F.; Alberti, R.; Frizzi, T.; Comelli, D. *Anal. Methods* **2014**, *6* (1), 130–138.

(21) Rosi, F.; Grazia, C.; Gabrieli, F.; Romani, A.; Paolantoni, M.; Vivani, R.; Brunetti, B. G.; Colomban, P.; Miliani, *Microchem. J.* **2016**, *124*, 856–867.

(22) Grazia, C.; Rosi, F.; Gabrieli, F.; Romani, A.; Paolantoni, M.; Vivani, R.; Brunetti, B. G.; Colomban, P.; Miliani, C. *Microchem. J.* **2016**, *125*, 279–289.

(23) Giacopetti, L.; Satta, A. *Microchem. J.* **2016**, *126*, 214–219.

(24) Mosca, S.; Frizzi, T.; Pontone, M.; Alberti, R.; Bombelli, L.; Capogrosso, V.; Nevin, A.; Valentini, G.; Comelli, D. *Microchem. J.* **2016**, *124*, 775–784.

(25) RRUFF Project website. http://rruff.info (2018)

(26) Raman Spectroscopic Library. http://www.chem.uc.ac.uk/resources/raman (2018)

(27) Artesani, A.; Bellei, S.; Capogrosso, V.; Cesaratto, A.; Mosca, S.; Nevin, A.; Valentini, G.; Comelli, D.

Appl. Phys. A Mater. Sci. Process. **2016**, *122* (12).

(28) Maspero, A.; Giovenzana, G. B.; Masciocchi, N.; Palmisano, G.; Comotti, A.; Sozzani, P.; Bassanetti, I.; Nardo, L. *Cryst. Growth Des.* **2013**, *13* (11), 4948–4956.

(29) Comelli, D.; Nevin, A.; Valentini, G.; Osticioli, I.; Castellucci, E. M.; Toniolo, L.; Gulotta, D.; Cubeddu, R. *J. Cult. Herit.* **2011**, *12* (1), 11–18.

(30) Haque, S. E.; Ramdas, B.; Sheela, A.; Padmavathy, N. *Micro & Nano Lett.* **2014**, *9* (10), 731–735.

(31) Chi, T. T. K.; Gouadec, G.; Colomban, P.; Wang, G.; Mazerolles, L.; Liem, N. Q. *J. Raman Spectrosc.* **2011**, *42* (5), 1007–1015.

(32) Thoury, M.; Delaney, J. K.; De La Rie, E. R.; Palmer, M.; Morales, K.; Krueger, J. *Appl. Spectrosc.* **2011**, *65* (8), 939–951.

FOR TOC ONLY